AN ELASTO-PLASTIC DYNAMIC CONSTITUTIVE MODEL BASED ON SUB-LOADING SURFACE THEORY AND APPLICATION ON SOIL LIQUEFACTION

L.Y. Li, X.L. Du and L. Li

The Key Lab. of Urban Security and Disaster Engineering (Ministry of Education), Beijing University of Technology, Beijing, P.R. China
Email: lly@bjut.edu.cn, duxl@iwhr.com

ABSTRACT :

It is known that the interior of the yield surface is a purely elastic domain for the conventional plastic constitutive equation. So, it is incapable of describing the plastic deformation due to the change of stress inside the yield surface (Drucker, 1988). Sub-loading surface theory assumes that the sub-loading surface always passes through the current stress point and also keeps the similar shape to the yield surface (Hashiguchi, 1980), and it expands/contracts with the plastic deformation. So, it can be extended to the description of cyclic loading behavior as has been done by Hashiguchi (1989) and by Hashiguchi and Yoshimaru (1995) for metals and by Topolnicki (1990), by Hashiguchi and Chen (1998) , by L. KONG, Y.R. ZHENG and Y.P. YAO (2003a,b) for soils. In this paper, based on sub-loading surface theory, an elasto-plastic model for dynamic constitutive relation of soil is deduced. The model is tested with the dynamic triaxial tests of sand. Then, the model is used to analyzing soil liquefaction by compiled to an explicit numerical wave method, which is based on soil mechanic model of fluid-saturated porous media theory and combined with viscous-spring artificial boundary. Finally, a soil liquefaction example induced earthquake is analyzed.

KEYWORDS: Sub-loading surface theory, Soil dynamic constitutive relation, Explicit numerical wave method, Soil liquefaction

1. INTRODUCTION

It is well known that earthquake maybe cause severe damage to country economy and life security. For example, the 1995 Hyogo-ken Nanbu (Kobe) earthquake brought about enormous damage to structures in the Hanshin and Awaji areas; the 1999 Kocaeli earthquake caused extensive liquefaction-induced ground deformations along the coasts of Sapanca Lake; the 1999 Chi-Chi, Taiwan earthquake caused great destruction to buildigs, bridges, and other facilities, and a death toll of more than 2400. In these earthquakes, a major cause for the damages is the foundation's invalidation. Under a dynamic loading (such as earthquake), the characteristics of soils can be changed. So, it is very important that the characterization of soil behavior is simulated accurately.

The purpose of a constitutive model is to simulate the soil behavior with sufficient accuracy under all loading conditions. There are many constitutive models describing soil's properties, such as Duncan-Chang elastic model, Prandtl-Reuss plastic model, Drucker-Prager model, Mohr-Coulomb model, Cam clay model, Lade-Duncan model, and Dafalias-Herrmann bounding surface model, and so on. And the elasto-plastic constitutive model is important in using. But, the interior of the yield surface is a purely elastic domain for the conventional plastic constitutive equation, it is incapable of describing the plastic deformation due to the change of stress inside the yield surface (Drucker, 1988). Then, it cannot describe the unloading properties of soils accurately.

Sub-loading surface theory assumes that the Sub-loading surface always passes through the current stress point and also keeps the similar shape to the yield surface (Hashiguchi, 1980), and it expands/contracts with the plastic deformation. So, it can be extended to the description of cyclic dynamic loading behavior as has been done by Hashiguchi (1988, 1989) and by Hashiguchi and Yoshimaru (1995) for metals and by Topolnicki (1990), by Hashiguchi (1998,2002,2003) , by L. KONG, Y.R. ZHENG and Y.P. YAO (2003a,b) for soils. In

this paper, based on sub-loading surface theory, an elasto-plastic model for dynamic constitutive relation of soil is deduced. And the model is tested with the dynamic triaxial tests of sands. Then, the model is used to analyzing soil liquefaction by compiled to an explicit numerical wave method (LI., 2007), which is based on soil mechanic model of fluid-saturated porous media theory and combined with viscous-spring artificial boundary (Du and Li., 2008). Finally, a soil liquefaction example induced by earthquake is analyzed.

2. AN ELASTO-PLASTIC DYNAMIC CONSTITUTIVE MODEL BASED ON SUB-LOADING SURFACE THEORY

2.1. Formulation of dynamic constitutive model

From Hashiguchi's works (Hashiguchi, 1980, 1989), we know that the Sub-loading surface theory can describe the plastic strain rate due to the rate of stress inside the yield surface. It is assumed that the plastic strain rate progresses as the ratio of the size of the Sub-loading surface to that of the yield surface increases, so, it is used to simulate cyclic loading behavior of soils.

In Sub-loading surface theory, the yield surface in the conventional sense is renamed the normal-yield surface in order to express its physical meaning clearly, and there is a Sub-loading surface which expands/contracts existing inside the normal-yield surface, passing always through a current stress point in not only a loading but also an unloading process and keeping a similarity to the normal-yield surface (Figure 1). Now, in this section, an elasto-plastic dynamic constitutive model based on Sub-loading surface theory is formulated concretely for soils incorporating the modified elliptic-hyperbolic yield surfaces model (M.Y. ZHANG, 1994; Z.Z YIN, 1996).

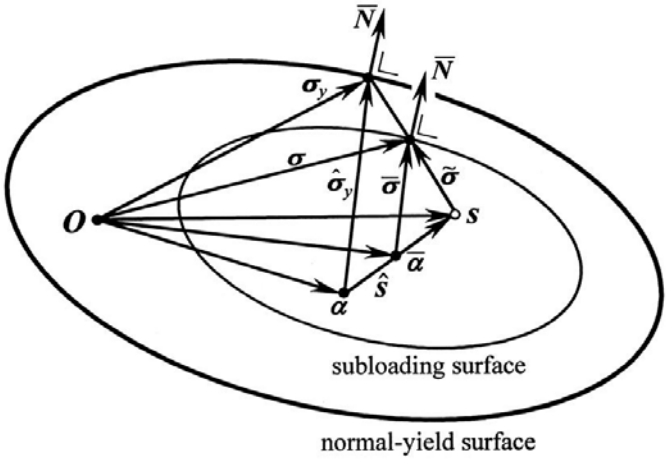

Figure 1 Normal-yield surface and Sub-loading surface (Hashiguchi, 1989)

The modified elliptic-hyperbolic yield surfaces model (Z.Z. YIN, 1996) assumes that the strain of soil include three parts, i.e. elastic stain, the plastic strain related to shear contraction, the plastic strain related to shear dilatation, and the strain which doesn't effect the volume change during shearing.

$$\{d\varepsilon\} = \{d\varepsilon^{e}\} + \{d\varepsilon^{p1}\} + \{d\varepsilon^{p2}\} + \{d\varepsilon^{p3}\} \tag{2.1}$$

where, $d\varepsilon^{e}$ represents the elastic strain; $d\varepsilon^{p1}$ represents the plastic strain related to shear contraction, and reflected with elliptic yield surface; $d\varepsilon^{p2}$ represents the plastic stain related to shear dilatation, reflected with hyperbolic yield surface; $d\varepsilon^{p3}$ represents the plastic strain which doesn't effect the volume change during shearing, submit to the generalized Hooke's law.

The first yield rule f_1 to reflect $d\varepsilon^{p1}$ is written as:

$$p + \frac{q^2}{M_1^{\,2}(p + p_r)} = p_0 = F(\varepsilon_v^{\,p}) = \frac{h\varepsilon_v^{\,p}}{1 - t\varepsilon_v^{\,p}} p_a \tag{2.2}$$

where, $p=(\sigma_1+\sigma_2+\sigma_3)/3=(\sigma_x+\sigma_y+\sigma_z)/3$;

$$q=\frac{1}{\sqrt{2}}\sqrt{(\sigma_1-\sigma_2)^2+(\sigma_2-\sigma_3)^2+(\sigma_3-\sigma_1)^2}$$
$$=\frac{1}{\sqrt{2}}\sqrt{(\sigma_x-\sigma_y)^2+(\sigma_y-\sigma_z)^2+(\sigma_z-\sigma_x)^2+6\tau_{xy}^{\ 2}+6\tau_{yz}^{\ 2}+6\tau_{zx}^{\ 2}};$$

p_r and M are the intercept and slope coefficient of the failure line q_f-p on the axis p, respectively, $p_r=c\cot\varphi$, $M=6\sin\varphi/(3-\sin\varphi)$; M_1 is a parameter larger than M, which has relation to the shape of stress-strain curve; c and φ are the parameters of Duncan-Chang elastic model; h and t are the hardening parameters; ε_v^p is plastic volume strain.

The second yield rule f_2 modified by M.Y. ZHANG (1994) to reflect $d\varepsilon^{p2}$ is:

$$\frac{q^2}{3G[M_2(p+p_r)-q]}=F(\varepsilon_s^{\ p})=\varepsilon_s^{\ p} \tag{2.3}$$

where,

$$\varepsilon_s^{\ p}=\int d\varepsilon_s^{\ p}=\int\frac{\sqrt{2}}{3}\sqrt{(d\varepsilon_1^{\ p}-d\varepsilon_2^{\ p})^2+(d\varepsilon_2^{\ p}-d\varepsilon_3^{\ p})^2+(d\varepsilon_3^{\ p}-d\varepsilon_1^{\ p})^2}$$
$$=\int\frac{\sqrt{2}}{3}\sqrt{(d\varepsilon_x^p-d\varepsilon_y^p)^2+(d\varepsilon_y^p-d\varepsilon_z^p)^2+(d\varepsilon_z^p-d\varepsilon_x^p)^2+3\times(d\gamma_{xy}^{p\ 2}+d\gamma_{yz}^{p\ 2}+d\gamma_{zx}^{p\ 2})/2}$$

$M_2=M/R_f$, R_f is the failure ratio of Duncan-Chang elastic model; $G=E/(2+2\nu)$, $E=(1.2\sim3.0)E_i$, and E_i is the initial elastic modular.

The third plastic strain submits to the generalized Hooke's law, then, it is integrated with the elastic strain during calculation, and expressing:

$$\{d\varepsilon^{'}\}=\{d\varepsilon^{e}\}+\{d\varepsilon^{p3}\} \tag{2.4}$$

where, the elastic modular is changed as

$$E^{'}=2kp_a\left(\frac{\sigma_3}{p_a}\right)^n\left[1-\frac{0.8(1-\sin\varphi)(\sigma_1-\sigma_3)}{2c\cos\varphi+2\sigma_3\sin\varphi}\right]^2 \tag{2.5}$$

k and n are also the parameters of Duncan-Chang elastic model.

The third plastic strain will be initiated while the stresses satisfy the second yield rule and $q>q_0$, which q_0 is the maximal shear stress in history.

Then, the Normal-yield surface is expressed as

$$f_1(\hat{\boldsymbol{\sigma}})=p+\frac{q^2}{M_1^{\ 2}(p+p_r)} \qquad F_1(\varepsilon_v^{\ p})=\frac{h\varepsilon_v^{\ p}}{1-t\varepsilon_v^{\ p}}p_a$$
$$f_2(\hat{\boldsymbol{\sigma}})=\frac{q^2}{3G[M_2(p+p_r)-q]} \qquad F_2(\varepsilon_s^{\ p})=\varepsilon_s^{\ p}$$

where, $\hat{\boldsymbol{\sigma}}=\boldsymbol{\sigma}-\boldsymbol{\alpha}$, the second-order tensor $\boldsymbol{\alpha}$ is the kinematic hardening variable, and $\boldsymbol{\sigma}$ is the current stress point.

According to Hashiguchi's works, there are the following relations

$$\overline{\boldsymbol{\sigma}}=\boldsymbol{\sigma}-\overline{\boldsymbol{\alpha}}=\boldsymbol{\sigma}-(1-R)\mathbf{s}-R\boldsymbol{\alpha},\quad \hat{\boldsymbol{\sigma}}=\overline{\boldsymbol{\sigma}}/R=\mathbf{s}-\boldsymbol{\alpha}+(\boldsymbol{\sigma}-\mathbf{s})/R,\quad \overline{\boldsymbol{\alpha}}=\mathbf{s}-R(\mathbf{s}-\boldsymbol{\alpha}) \tag{2.6}$$

where, R is the normal-subloading ratio, which is the ratio of the size of the sub-loading surface to that of the normal-yield surface, $0\le R\le1$. $R=0$ corresponds to the most elastic state where $\boldsymbol{\sigma}$ coincides with $\boldsymbol{\alpha}$, and $R=1$ corresponds to the normal-yield state where $\boldsymbol{\sigma}$ lies on the normal-yield surface; $\mathbf{s}$ is the similarity-center that exists for the specified configuration of the normal-yield and the sub-loading surfaces.

For the first two yield surface, we suppose that the coordinate of the similarity-center are $(s_v^{\ p}, s_v^{\ q})$ and $(s_s^{\ p}, s_s^{\ q})$, respectively; and the center point lie in the origin of the $p-q$ coordinate system. The following relations hold:

$$\bar{p}_v = p-(1-R_v)s_v^{\ p},\ \ \bar{q}_v = q-(1-R_v)s_v^{\ q},\ \ \bar{p}_s = p-(1-R_s)s_s^{\ p},\ \ \bar{q}_s = q-(1-R_s)s_s^{\ q}$$

and the R_v and R_s are obtained respectively from

$$\bar{p}_v + \frac{\bar{q}_v^{\ 2}}{M_1^{\ 2}(\bar{p}_v + p_r)} = R_v p_0 = R_v F(\varepsilon_v^{\ p}) = R_v \frac{h\varepsilon_v^{\ p}}{1-t\varepsilon_v^{\ p}} p_a \tag{2.7}$$

and

$$\frac{\bar{q}_s^{\ 2}}{3G[M_2(\bar{p}_s + p_r) - \bar{q}_s]} = R_s \varepsilon_s^{\ p} \tag{2.8}$$

The expressions are

$$R_v = \frac{-b+\sqrt{b^2-4ac}}{2a} \tag{2.9}$$

where, $a = M_1^{\ 2}s_v^{p\,2} + s_v^{q\,2} - M_1^{\ 2}p_0 s_v^{p}$

$$b = -(2M_1^{\ 2}s_v^{p\,2} + 2s_v^{q\,2} - 2M_1^{\ 2}ps_v^{p} - M_1^{\ 2}p_r s_v^{p} - 2qs_v^{q} - M_1^{\ 2}p_0 s_v^{p} + M_1^{\ 2}p_0 p + M_1^{\ 2}p_0 p_r)$$

$$c = M_1^{\ 2}s_v^{p\,2} + s_v^{q\,2} - 2M_1^{\ 2}ps_v^{p} - M_1^{\ 2}p_r s_v^{p} - 2qs_v^{q} + M_1^{\ 2}p_r p + q^2 + M_1^{2}p^2$$

$$R_s = \frac{-b^{'}+\sqrt{b^{'2}-4a^{'}c^{'}}}{2a^{'}} \tag{2.10}$$

where, $a^{'} = 3G\varepsilon_s^{p}s_s^{q} + s_s^{q\,2} - 3GM_2\varepsilon_s^{\mathrm{p}}s_s^{p}$

$$b^{'} = 2qs_s^{q} - 2s_s^{q\,2} - 3GM_2(p+p_r)\varepsilon_s^{\mathrm{p}} + 3GM_2\varepsilon_s^{\mathrm{p}}s_s^{p} + 3Gq\varepsilon_s^{\mathrm{p}} - 3G\varepsilon_s^{\mathrm{p}}s_s^{q}$$

$$c^{'} = q^2 + s_s^{q\,2} - 2qs_s^{q} = (q-s_s^{q})^2$$

Based on the two yield rules, the evolvements of the two similarity-centers and normal-subloading ratios are formulated, which are

$$\mathrm{d}s_{vi} = \frac{\mathrm{d}F_v}{F_v}s_{vi} + \frac{c_v}{R_v}\mathrm{d}\varepsilon_v^{\ \mathrm{p}}(\sigma_i - s_{vi}),\ \ \mathrm{d}s_{si} = \frac{\mathrm{d}F_s}{F_s}s_{si} + \frac{c_s}{R_s}\mathrm{d}\varepsilon_s^{\ \mathrm{p}}(\sigma_i - s_{si})$$

$$\mathrm{d}R_v = -u_v\mathrm{d}\varepsilon_v^{\ \mathrm{p}}\ln R_v,\ \ \mathrm{d}R_s = -u_s\mathrm{d}\varepsilon_s^{\ \mathrm{p}}\ln R_s$$

$$F_v = F_1(\varepsilon_v^{\ \mathrm{p}}),\ \ F_s = F_2(\varepsilon_s^{\ \mathrm{p}}),\ \ \mathrm{d}F_v = \frac{hp_a}{(1-t\varepsilon_v^{\ \mathrm{p}})^2}\mathrm{d}\varepsilon_v^{\ \mathrm{p}},\ \ \mathrm{d}F_s = \mathrm{d}\varepsilon_s^{\ \mathrm{p}}$$

where, c_v、c_s、u_v、u_s are the material constants; R_v and R_s are the volume normal-subloading ratio and the shear normal-subloading ratio.

Finally, the relations are formulated as

$$\begin{Bmatrix}\mathrm{d}\varepsilon_v^{\ \mathrm{p}}\\ \mathrm{d}\varepsilon_s^{\ \mathrm{p}}\end{Bmatrix} = \begin{bmatrix}\beta_1 & \beta_2\\ \beta_3 & \beta_4\end{bmatrix}\begin{Bmatrix}\mathrm{d}p\\ \mathrm{d}q\end{Bmatrix} \tag{2.11}$$

where, the expressions of $\beta_1, \beta_2, \beta_3, \beta_4$ can be seen in references(Li, 2007).

The loading criterion is

$$\left.\begin{aligned}\mathrm{d}\boldsymbol{\varepsilon}^{\mathrm{p}} \neq 0 : \mathrm{tr}(\bar{\mathbf{N}}\mathbf{D}\mathrm{d}\boldsymbol{\varepsilon}) > 0\\ \mathrm{d}\boldsymbol{\varepsilon}^{\mathrm{p}} = 0 : \mathrm{tr}(\bar{\mathbf{N}}\mathbf{D}\mathrm{d}\boldsymbol{\varepsilon}) \le 0\end{aligned}\right\} \tag{2.12}$$

where, $\overline{\mathbf{N}} = \dfrac{\partial f(\overline{\boldsymbol{\sigma}})}{\partial \overline{\boldsymbol{\sigma}}} \Big/ \left\| \dfrac{\partial f(\overline{\boldsymbol{\sigma}})}{\partial \overline{\boldsymbol{\sigma}}} \right\| = \hat{\mathbf{N}} = \dfrac{\partial f(\hat{\boldsymbol{\sigma}})}{\partial \hat{\boldsymbol{\sigma}}} \Big/ \left\| \dfrac{\partial f(\hat{\boldsymbol{\sigma}})}{\partial \hat{\boldsymbol{\sigma}}} \right\|$

2.2. Test verification by Dynamic triaxial test

Dynamic triaxial tests of sands were carried through in the soil mechanic laboratory of Beijing University of Technology. They are un-drained dynamic triaxial test, under several concretion pressures. The typical dynamic triaxial test records are shown in Figure 2, and Figure 3 is the simulation result of the axial strain history with the proposed model, with the axial stress and pore pressure are independent variable of calculating. From the result, we can see that it is good agreement between experiment and simulation result.

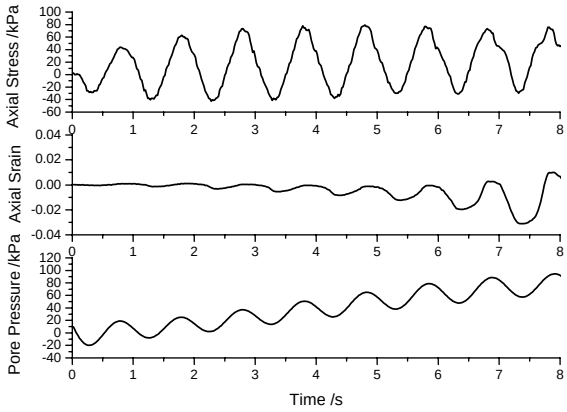

Figure 2 The history of the dynamic triaxial test

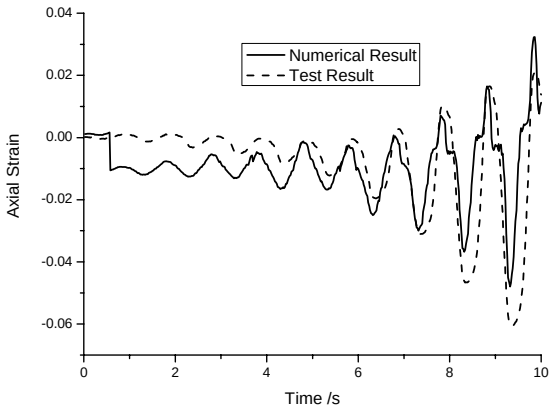

Figure 3 The axial strain history from the test and simulation result with the model

3. NONLINEAR EXPLICIT FEM TO ANALYZE THE WAVE PROPAGATION IN SATURATED POROUS MEDIA

The formulations of the soil mechanics model to analyze the wave propagation in saturated porous media include

$$\begin{aligned} \sigma_{ij,i} + (1-n)\sigma^{\mathrm{f}}_{,i} + b_i\left(V_{i,t} - U_{i,t}\right) + (1-n)\rho_{\mathrm{s}} g_i &= (1-n)\rho_{\mathrm{s}} U_{i,tt} \\ n\sigma^{\mathrm{f}}_{,i} - b_i\left(V_{i,t} - U_{i,t}\right) + n\rho_{\mathrm{f}} g_i &= n\rho_{\mathrm{f}} V_{i,tt} \\ \sigma^{\mathrm{s}}_{ij} &= (\lambda\varepsilon + \alpha\sigma^{\mathrm{f}})\delta_{ij} + 2G\varepsilon_{ij} \\ (1-n)\mathrm{div}\dot{\boldsymbol{U}} + n\mathrm{div}\dot{\boldsymbol{V}} - \frac{n}{E_{\mathrm{f}}}\sigma^{\mathrm{f}}_{,t} &= 0 \\ b_i &= \frac{n^2\rho_{\mathrm{f}} g}{K_i} \end{aligned} \tag{3.1}$$

Using the finite element reduction and decoupling technique, the dynamic equilibrium equations of one nodal point are written as

$$M_{si}\mathrm{d}\ddot{\boldsymbol{U}}_i + \sum_{L=1}^{8(4)}\sum_{j=1}^{8}\left(C^L_{\mathrm{ssk}(i)j}\mathrm{d}\dot{\boldsymbol{U}}^L_j - C^L_{\mathrm{sfk}(i)j}\mathrm{d}\dot{\boldsymbol{V}}^L_j + K^L_{\mathrm{ssk}(i)j}\mathrm{d}\boldsymbol{U}^L_j + K^L_{\mathrm{sfk}(i)j}\mathrm{d}\boldsymbol{V}^L_j\right) - M_{ti}\boldsymbol{G}_i = \mathrm{d}\boldsymbol{P}_{\mathrm{si}} \tag{3.2}$$

$$M_{\mathrm{fi}}\mathrm{d}\ddot{\boldsymbol{V}}_i + \sum_{L=1}^{8(4)}\sum_{j=1}^{8}\left(-C^L_{\mathrm{fsk}(i)j}\mathrm{d}\dot{\boldsymbol{U}}^L_j + C^L_{\mathrm{ffk}(i)j}\mathrm{d}\dot{\boldsymbol{V}}^L_j + K^L_{\mathrm{fsk}(i)j}\mathrm{d}\boldsymbol{U}^L_j + K^L_{\mathrm{ffk}(i)j}\mathrm{d}\boldsymbol{V}^L_j\right) = \mathrm{d}\boldsymbol{P}_{\mathrm{fi}} \tag{3.3}$$

where, M_{si} , M_{fi} and M_{ti} are the solid mass, fluid mass, and total mass of the nodal point i ;

$C^L_{\mathrm{ssk}(i)j}, C^L_{\mathrm{sfk}(i)j}, C^L_{\mathrm{fsk}(i)j}, C^L_{\mathrm{ffk}(i)j}$ are damp matrix of element L, and $K^L_{\mathrm{ssk}(i)j}$, $K^L_{\mathrm{sfk}(i)j}$, $K^L_{\mathrm{fsk}(i)j}$, $K^L_{\mathrm{ffk}(i)j}$ are stiffness matrix of element L; $\mathrm{d}\boldsymbol{U}_j$ and $\mathrm{d}\boldsymbol{V}_j$ are the displacement increment vectors; $\boldsymbol{G}_j$ is the gravity vector; $\mathrm{d}\boldsymbol{P}_{\mathrm{s}j}$ and $\mathrm{d}\boldsymbol{P}_{\mathrm{f}j}$ are the loading increment vectors.

Employing an explicit time integration proposed by J.T. WANG(2001), the following formulations are gained

$$\begin{aligned}
\mathrm{d}\boldsymbol{U}_i^{p+1} &= \mathrm{d}\boldsymbol{U}_i^{p} + \mathrm{d}\dot{\boldsymbol{U}}_i^{p}\Delta t \\
&\quad -\frac{\Delta t}{2} M_{\mathrm{s}i}^{-1} \sum_L \sum_j C^L_{\mathrm{ssk}(i)j} [2(\mathrm{d}\dot{\boldsymbol{U}}_j^{p})^L \Delta t + (\mathrm{d}\boldsymbol{U}_j^{p-1})^L - (\mathrm{d}\boldsymbol{U}_j^{p})^L] \\
&\quad +\frac{\Delta t}{2} M_{\mathrm{s}i}^{-1} \sum_L \sum_j C^L_{\mathrm{sfk}(i)j} [2(\mathrm{d}\dot{\boldsymbol{V}}_j^{p})^L \Delta t + (\mathrm{d}\boldsymbol{V}_j^{p-1})^L - (\mathrm{d}\boldsymbol{V}_j^{p})^L] \\
&\quad -\frac{\Delta t^2}{2} M_{\mathrm{s}i}^{-1} \sum_L \sum_j K^L_{\mathrm{ssk}(i)j} (\mathrm{d}\boldsymbol{U}_j^{p})^L \\
&\quad -\frac{\Delta t^2}{2} M_{\mathrm{s}i}^{-1} \sum_L \sum_j K^L_{\mathrm{sfk}(i)j} (\mathrm{d}\boldsymbol{V}_j^{p})^L + \frac{\Delta t^2}{2} M_{\mathrm{s}i}^{-1} M_{\mathrm{t}i} \boldsymbol{G}_i + \frac{\Delta t^2}{2} M_{\mathrm{s}i}^{-1} \mathrm{d}\boldsymbol{P}_{\mathrm{s}i}^{p}
\end{aligned} \tag{3.4a}$$

$$\begin{aligned}
\mathrm{d}\boldsymbol{V}_i^{p+1} &= \mathrm{d}\boldsymbol{V}_i^{p} + \mathrm{d}\dot{\boldsymbol{V}}_i^{p}\Delta t \\
&\quad -\frac{\Delta t}{2} M_{\mathrm{f}i}^{-1} \sum_L \sum_j C^L_{\mathrm{ffk}(i)j} [2(\mathrm{d}\dot{\boldsymbol{V}}_j^{p})^L \Delta t + (\mathrm{d}\boldsymbol{V}_j^{p-1})^L - (\mathrm{d}\boldsymbol{V}_j^{p})^L] \\
&\quad +\frac{\Delta t}{2} M_{\mathrm{f}i}^{-1} \sum_L \sum_j C^L_{\mathrm{fsk}(i)j} [2(\mathrm{d}\dot{\boldsymbol{U}}_j^{p})^L \Delta t + (\mathrm{d}\boldsymbol{U}_j^{p-1})^L - (\mathrm{d}\boldsymbol{U}_j^{p})^L] \\
&\quad -\frac{\Delta t^2}{2} M_{\mathrm{f}i}^{-1} \sum_L \sum_j K^L_{\mathrm{ffk}(i)j} (\mathrm{d}\boldsymbol{V}_j^{p})^L \\
&\quad -\frac{\Delta t^2}{2} M_{\mathrm{f}i}^{-1} \sum_L \sum_j K^L_{\mathrm{fsk}(i)j} (\mathrm{d}\boldsymbol{U}_j^{p})^L + \frac{\Delta t^2}{2} M_{\mathrm{f}i}^{-1} \mathrm{d}\boldsymbol{P}_{\mathrm{f}i}^{p}
\end{aligned} \tag{3.4b}$$

$$\begin{aligned}
\mathrm{d}\dot{\boldsymbol{U}}_i^{p+1} &= -\frac{1}{2} M_{\mathrm{s}i}^{-1} \sum_L \sum_j C^L_{\mathrm{ssk}(i)j} \left[(\mathrm{d}\boldsymbol{U}_j^{p+1})^L - (\mathrm{d}\boldsymbol{U}_j^{p})^L\right] \\
&\quad +\frac{1}{2} M_{\mathrm{s}i}^{-1} \sum_L \sum_j C^L_{\mathrm{sfk}(i)j} \left[(\mathrm{d}\boldsymbol{V}_j^{p+1})^L - (\mathrm{d}\boldsymbol{V}_j^{p})^L\right] - \\
&\quad \frac{\Delta t}{2} M_{\mathrm{s}i}^{-1} \sum_L \sum_j K^L_{\mathrm{ssk}(i)j} (\mathrm{d}\boldsymbol{U}_j^{p+1})^L - \frac{\Delta t}{2} M_{\mathrm{s}i}^{-1} \sum_L \sum_j K^L_{\mathrm{sfk}(i)j} (\mathrm{d}\boldsymbol{V}_j^{p+1})^L \\
&\quad +\frac{\Delta t}{2} M_{\mathrm{s}i}^{-1} M_{\mathrm{t}i} \boldsymbol{G}_i + \frac{1}{\Delta t} \left[\mathrm{d}\boldsymbol{U}_i^{p+1} - \mathrm{d}\boldsymbol{U}_i^{p}\right] + \frac{\Delta t}{2} M_{\mathrm{s}i}^{-1} \mathrm{d}\boldsymbol{P}_{\mathrm{s}i}^{p+1}
\end{aligned} \tag{3.4c}$$

$$
\begin{aligned}
\mathrm{d}\dot{\boldsymbol{V}}_i^{p+1} = & -\frac{1}{2}M_{\mathrm{f}i}^{-1}\sum_L\sum_j C_{\mathrm{ff}k(i)j}^L\left[(\mathrm{d}\boldsymbol{V}_j^{p+1})^L-(\mathrm{d}\boldsymbol{V}_j^{p})^L\right] \\
& +\frac{1}{2}M_{\mathrm{f}i}^{-1}\sum_L\sum_j C_{\mathrm{fs}k(i)j}^L\left[(\mathrm{d}\boldsymbol{U}_j^{p+1})^L-(\mathrm{d}\boldsymbol{U}_j^{p})^L\right] \\
& -\frac{\Delta t}{2}M_{\mathrm{f}i}^{-1}\sum_L\sum_j K_{\mathrm{ff}k(i)j}^L(\mathrm{d}\boldsymbol{V}_j^{p+1})^L-\frac{\Delta t}{2}M_{\mathrm{f}i}^{-1}\sum_L\sum_j K_{\mathrm{fs}k(i)j}^L(\mathrm{d}\boldsymbol{U}_j^{p+1})^L \\
& +\frac{1}{\Delta t}\left[\mathrm{d}\boldsymbol{V}_i^{p+1}-\mathrm{d}\boldsymbol{V}_i^{p}\right]+\frac{\Delta t}{2}M_{\mathrm{f}i}^{-1}\mathrm{d}\boldsymbol{P}_{\mathrm{f}i}^{p+1}
\end{aligned}
\tag{3.4d}
$$

Combining with a viscous-spring artificial boundary in near-field wave propagation analysis of saturated porous media (DU & LI, 2008), the formula (3.2) to (3.3) are changed as

$$
\begin{aligned}
M_{\mathrm{s}i}\mathrm{d}\ddot{\boldsymbol{U}}_i+\sum_L\sum_j(C_{\mathrm{ss}k(i)j}^L\mathrm{d}\dot{\boldsymbol{U}}_j^L-C_{\mathrm{sf}k(i)j}^L\mathrm{d}\dot{\boldsymbol{V}}_j^L)+\sum_L\sum_j(K_{\mathrm{ss}k(i)j}^L\mathrm{d}\boldsymbol{U}_j^L+K_{\mathrm{sf}k(i)j}^L\mathrm{d}\boldsymbol{V}_j^L) & \\
-M_{\mathrm{t}i}\boldsymbol{G}_i+\sum_L S_{k(i)}^L\overline{K}_{\mathrm{ss}k(i)k(i)}^L\mathrm{d}\boldsymbol{U}_{k(i)}^L+\sum_L S_{k(i)}^L\overline{C}_{\mathrm{ss}k(i)k(i)}^L\mathrm{d}\dot{\boldsymbol{U}}_{k(i)}^L & \\
=\mathrm{d}\boldsymbol{f}_{\mathrm{s}i}^{\mathrm{F}}(t)+\sum_L S_{k(i)}^L\overline{K}_{\mathrm{ss}k(i)k(i)}^L\mathrm{d}\boldsymbol{U}_{k(i)}^{L\ \mathrm{F}}+\sum_L S_{k(i)}^L\overline{C}_{\mathrm{ss}k(i)k(i)}^L\mathrm{d}\dot{\boldsymbol{U}}_{k(i)}^{L\ \mathrm{F}} &
\end{aligned}
\tag{3.5}
$$

$$
\begin{aligned}
M_{\mathrm{f}i}\mathrm{d}\ddot{\boldsymbol{V}}_i+\sum_L\sum_j(-C_{\mathrm{fs}k(i)j}^L\mathrm{d}\dot{\boldsymbol{U}}_j^L+C_{\mathrm{ff}k(i)j}^L\mathrm{d}\dot{\boldsymbol{V}}_j^L)+\sum_L\sum_j(K_{\mathrm{fs}k(i)j}^L\mathrm{d}\boldsymbol{U}_j^L+K_{\mathrm{ff}k(i)j}^L\mathrm{d}\boldsymbol{V}_j^L) & \\
+\sum_L S_{k(i)}^L\overline{K}_{\mathrm{ff}k(i)k(i)}^L\mathrm{d}\boldsymbol{V}_{k(i)}^L+\sum_L S_{k(i)}^L\overline{C}_{\mathrm{ff}k(i)k(i)}^L\mathrm{d}\dot{\boldsymbol{V}}_{k(i)}^L & \\
=\mathrm{d}\boldsymbol{f}_{\mathrm{f}i}^{\mathrm{F}}(t)+\sum_L S_{k(i)}^L\overline{K}_{\mathrm{ff}k(i)k(i)}^L\mathrm{d}\boldsymbol{V}_{k(i)}^{L\ \mathrm{F}}+\sum_L S_{k(i)}^L\overline{C}_{\mathrm{ff}k(i)k(i)}^L\mathrm{d}\dot{\boldsymbol{V}}_{k(i)}^{L\ \mathrm{F}} &
\end{aligned}
\tag{3.6}
$$

where, $\overline{K}_{\mathrm{ss}k(i)k(i)}$, $\overline{K}_{\mathrm{sf}k(i)k(i)}$, $\overline{C}_{\mathrm{ss}k(i)k(i)}$, $\overline{C}_{\mathrm{sf}k(i)k(i)}$ are the solid phase spring or damp parameters, and $\overline{K}_{\mathrm{fs}k(i)k(i)}$, $\overline{K}_{\mathrm{ff}k(i)k(i)}$, $\overline{C}_{\mathrm{fs}k(i)k(i)}$, $\overline{C}_{\mathrm{ff}k(i)k(i)}$ are the fluid phase spring or damp parameters in the viscous-spring artificial boundary; The superscript F represents the free site.

And then, the calculation formulations of boundary nodal point are gained which are similar to the formula (3.4a) to (3.4d).

4.ANALYSIS ON SOIL LIQUEFACTION

4.1. A method to distinguish soil liquefaction

There is a relation in soil mechanics $\tau=(\sigma-u)\tan\varphi$ (4.1)

So, the criterion of soil liquefaction is $u=\sigma$ (4.2)

In three stress-space, there is following relation $\tau_{\mathrm{oct}}^{\mathrm{f}}=(\sigma_{\mathrm{oct}}^{\mathrm{sd}}-u)\tan\varphi$ (4.3)

In the three dimension complex stress state, the earthquake force can be disintegrated into hydrostatic stress and deviatoric stress carried by pore water and soil skeleton in saturated soil, respectively. (Figure 4)

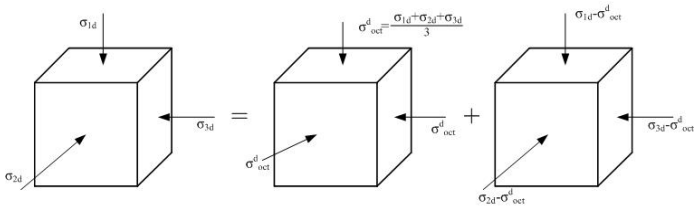

Total dynamic stress Hydrostatic stress Deviatoric stress

Figure 4 Analysis of the dynamic stress

There are the following octahedral dynamic normal stress and octahedral dynamic shear stress

$$\sigma_{\text{oct}}^{\text{d}} = \frac{1}{3}(\sigma_{1d} + \sigma_{2d} + \sigma_{3d}), \qquad \tau_{\text{oct}}^{\text{d}} = \frac{1}{3}\sqrt{(\sigma_{1d} - \sigma_{2d})^2 + (\sigma_{2d} - \sigma_{3d})^2 + (\sigma_{3d} - \sigma_{1d})^2}$$

Then, there exist the following criterion

$\tau_{\text{oct}}^{\text{d}} + \tau_{\text{oct}}^{\text{s}} < \tau_{\text{oct}}^{\text{f}}$, no liquefaction

$\tau_{\text{oct}}^{\text{d}} + \tau_{\text{oct}}^{\text{s}} \geq \tau_{\text{oct}}^{\text{f}}$, there are liquefaction trendency (4.4)

$\tau_{\text{oct}}^{\text{f}} = 0$, i.e. $\sigma_{\text{oct}}^{\text{sd}} = u$, liquefaction take place

The pore pressure ratio can be induced

$$\alpha_u = \frac{u}{\sigma_{\text{oct}}^{\text{sd}}} = \frac{u}{\sigma_{\text{oct}}^{\text{sd}'} + u} \tag{4.5}$$

if $\alpha_u = 1.0$, liquefaction will take place, and if $\alpha_u < 1.0$, there isn't liquefaction, but its value indicates the degree of liquefaction.

So, combining the above criterion to the FEM program, the soil liquefaction will be distinguished according the calculated stresses.

4.2 Soil liquefaction example

There is a free site, its layer is composed of top clay (Thickness d=2m, Shear modulus G=1.0×10^{7}Pa, Density ρ_s =2.0×10^{3}kg/m^3, Poisson's ratio ν =0.3, the strength index M=1.55, M_1=1.5, M_2=1.48, p_r=2100.0kPa, c=1642.0kPa, φ=38.0°, R_f=0.96, h=899.0, t=53.0, and parameters of sub-loading surface model c_v =4.0, c_s =4.0, u_v =50.0, u_s =30.0), middle saturated sand (Thickness d=8m, Compression modulus of Solid E_s =3.6×10^{9}Pa , Shear modulus G=1.0×10^{7}Pa, Density of solid grain ρ_s =2.0×10^{3}kg/m^3, Poisson's ratio ν =0.3, Porosity n=0.367, Density of fluid ρ_w =1.0×10^{3}kg/m^3, Volume compression modulus of fluid E_w =2.0×10^{8}Pa , Coefficient of permeability k_x=k_y=8.0×10^{-4}m/s, the strength index M=1.68, M_1=1.93, M_2=1.84, p_r=6.373kPa, c=5.44kPa, φ=41.0°, R_f=0.96, h=4400, t=1.88.0, and parameters of sub-loading surface model c_v =15.0、 c_s =15.5、 u_v =50.0、 u_s =30.0), and bottom clay (Thickness d=8m, Shear modulus G=1.5×10^{7}Pa, Density ρ_s =2.0×10^{3}kg/m^3, Poisson's ratio ν =0.3, the strength index M=1.55, M_1=1.5, M_2=1.48, p_r=2100.0kPa, c=1642.0kPa, φ=38.0°, R_f=0.96, h=899.0, t=53.0, and parameters of sub-loading surface model c_v =4.0, c_s =4.0, u_v =50.0, u_s =30.0).

The calculated area is a rectangle area whose size is 20.0m×18.0m, the element type is quadrilateral isoparametric element whose size is 2.0m. The input load is horizontal earthquake motion in plane which is inputted from the bottom of the area, whose time history of displacement, velocity and acceleration are showed in Figure 5 to 7. Figure 8 is the Fourier Spectrum of the input earthquake acceleration.

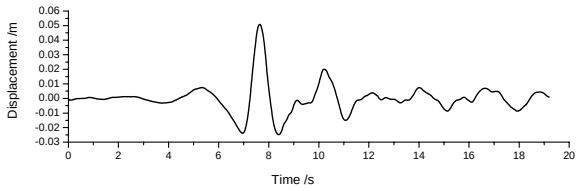

Figure 5 Displacement history of the input earthquake motion

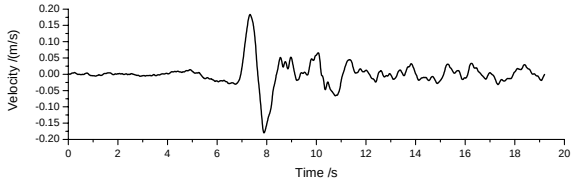

Figure 6 Displacement history of the input earthquake motion

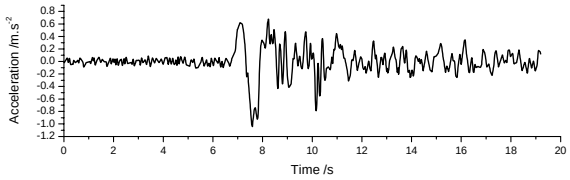

Figure7 Acceleration history of the input earthquake motion

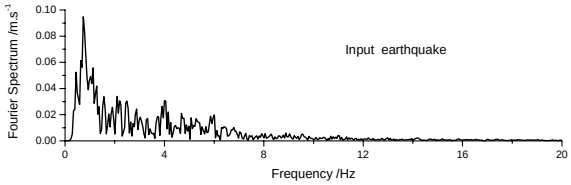

Figure 8 Fourier Spectrum of the input earthquake acceleration

The following figures are the calculated results. Figure 9 to 10 are the Solids horizontal displacements history and the Fluid horizontal displacements history in different depth, respectively. Figure 11 to 12 are the Solids horizontal velocity history and the Fluid horizontal velocity history in different depth, respectively. From the two former figures, we can see that the displacement amplitude of shallow layer is great than that of deep layer. From the two latter figures, it is known that the velocity amplitude also submits the same law.

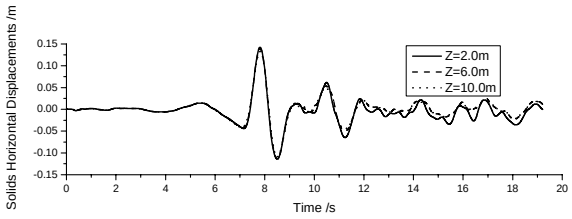

Figure 9 Solids horizontal displacements history in different depth

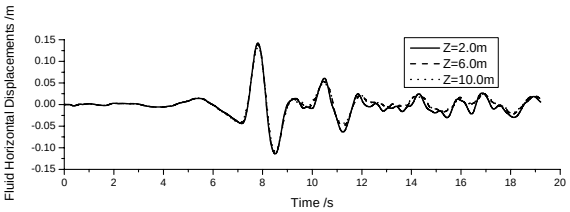

Figure 10 Fluid horizontal displacements history in different depth

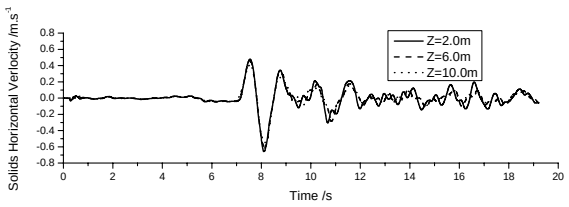

Figure 11 Solids Horizontal velocity history in different depth

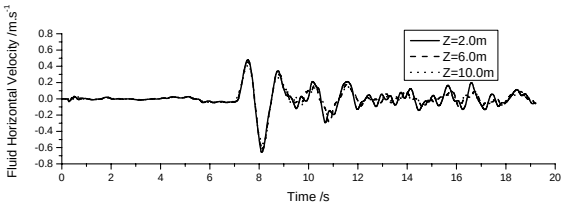

Figure 12 Fluid Horizontal velocity history in different depth

Compare the calculated Solids horizontal acceleration and its Fourier spectrum of the surface to the input horizontal acceleration and its Fourier spectrum (Figure 8 to 9, Figure 13 to 14), we know that the frequency component changes from wide to narrow, and the major frequency component of the surface is low frequency.

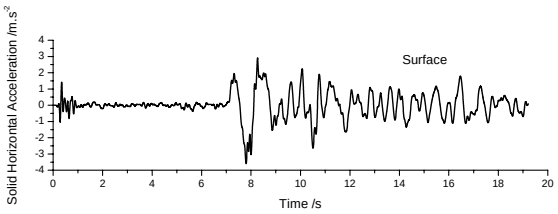

Figure 13 Solid Horizontal acceleration on surface

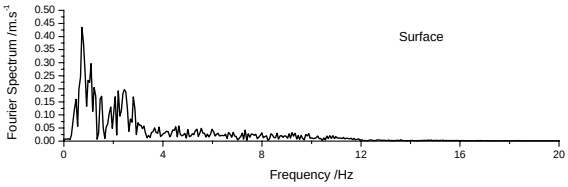

Figure 14 Fourier Spectrum of Solid Horizontal acceleration on surface

In order to analyze soil liquefaction of the site, the Pore Pressures and their corresponding Pore Pressure Ratio history are also studied (Figure 15 to16). From these results, it is concluded that (1) the pore pressure ratio history curves enlarge step by step and then keep gentle; (2) Pore pressure ratio of the shallow sand layer is greater than that of the deep layer, it indicates that the shallow sand layer's resistivity of liquefaction is small than the deep sand layer's.

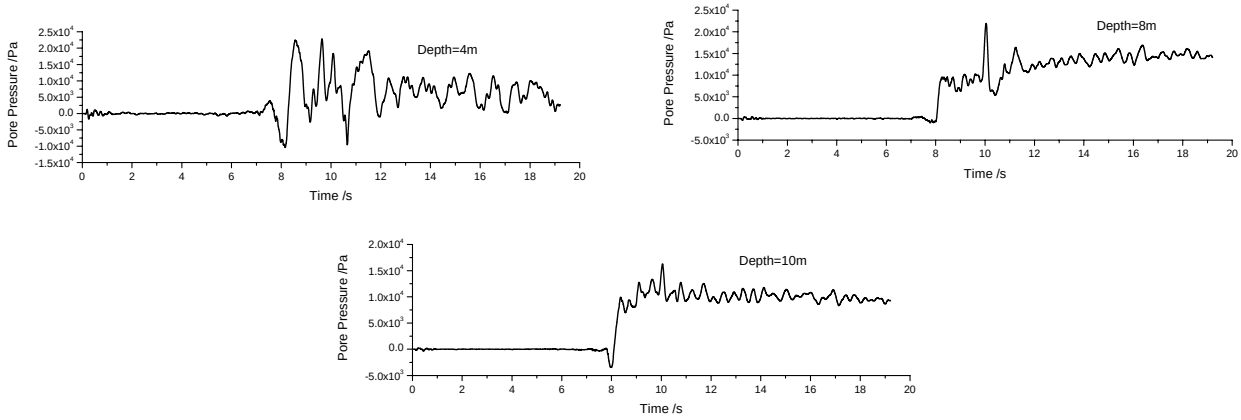

Fig.15 Pore Pressure history

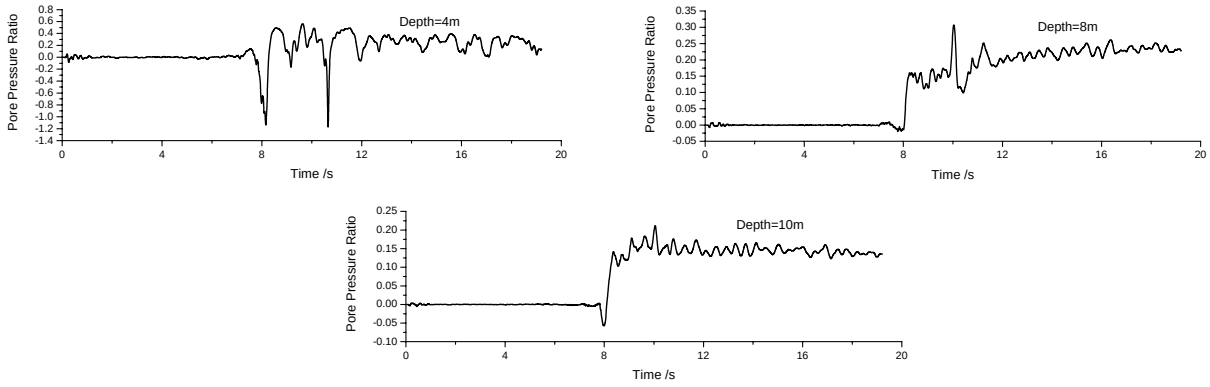

Fig.16 Pore Pressure Ratio history

5. CONCLUSION

In this paper, based on the sub-loading surface theory, an elasto-plastic model for dynamic constitutive relation of soil is deduced, and it is compiled to an explicit numerical wave method, which is based on soil mechanic model of fluid-saturated porous media theory and combined with viscous-spring artificial boundary. Then, integrating the suggested criterion of soil liquefaction, a method to analyze soil liquefaction is proposed. Finally, a soil liquefaction example under earthquake is analyzed.

ACKNOWLEDGEMENTS

This research has been supported by the National Natural Science Foundation of China (NSFC) under Grant No. 50508002 and No.50678002.

REFERENCES

Drucker, D.C. (1988). Conventional and unconventional plastic response and representation. *Appl. Mech. Rev. (ASME)* **41**, 151-167.

Hashiguchi, K. (1980). Constitutive equations of elastoplastic materials with elastic-plastic transition. *J. Appl. Mech. (ASME)* 47, 266-272.

Hashiguchi, K. (1988). A mathematical modification of two surface model formulation in plasticity. *Int. J. Solids Struct.* **24,** 987–1001.

Hashiguchi, K. (1989). Subloading surface model in unconventional plasticity. *Int. J. Solids Struct.* **25,** 917–945.

Hashiguchi, K., Yoshimaru, T., 1995. A generalized formulation of the concept of nonhardening region. *Int. J. Plasticity* **11,** 347–365.

Hashiguchi, K., Saitoh, K., Okayasu, T., Tsutsumi, S. (2002). Evaluation of typical conventional and unconventional plasticity models for prediction of softening behavior of soils. *Geotechnique* **52,** 561–573.

Hashiguchi, K., Tsutsumi, S. (2003). Shear band formation analysis in soils by the subloading surface model with tangential stress rate effect. *Int. J. Plasticity* **19**, 1651–1677.

J.T. WANG. (2001). The analyses of seismic response of high concrete dam-compressible water-sediment-foundation systems[D]. **Beijing**: *China Institute of Water Resources and Hydropower Research.*, (in Chinese)

K. Hashiguchi, Z.-P. Chen. (1998). Elastoplastic constitutive equation of soils with the subloading surface and the rotational hardening. *International Journal for numerical and analytical methods in geomechanics,* **22**, 197-227

L. KONG., Y.R. ZHENG, Y.P. YAO (2003a). Subloading surface cyclic plastic model for soil based on Generalized plasticity(I): Theory and model. *Rock and Soil Mechanics*, **24(2):** 141-145. (in Chinese)

L. KONG, Y.R. ZHENG, Y.P. YAO (2003b). Subloading surface cyclic plastic model for soil based on Generalized plasticity(II): Constitutive equation and identification. *Rock and Soil Mechanics,* **24(3):** 349-354. (in Chinese)

L.Y. LI (2007). Study on the non-linear dynamic interaction between quasi-saturated soil and substructure [D]. *Beijing: Beijing University of Technology.* (in Chinese)

M. Topolnicki (1990). An elasto-plastic subloading surface model for clay with isotropic and kinematic mixed hardening parameters. *Soils Found.*, **30,** 103-113.

M.Y. Zhang. (1994). A study of soil models with two yield surfaces. *Journal of Qingdao Institute of Architecture and Engineering*, **15(1):** 20-24. (in Chinese)

X.L. Du, L.Y. Li (2008). A viscous-spring artificial boundary for near-field wave analysis in saturated porous media. *Chinese J. Geophy.* **51(2):** 575-581. (in Chinese)

Z.Z. Yin, H.H. Lu, J.G. Zhu, 1996. The elliptic-parabolic yield surfaces model and its softness matrix. *SHULI XUEBAO,* **12,** 23-28. (in Chinese)